Observations of the impenetrable barrier, the plasmapause, and the VLF bubble during the 17 March 2015 storm

Citation: Foster, J. C.; Erickson, P. J.; Baker, D. N.; Jaynes, A. N.; Mishin, E. V.; Fennel, J. F.; Li, X.; Henderson, M. G. and Kanekal, S. G."Observations of the Impenetrable Barrier, the Plasmapause, and the VLF Bubble During the 17 March 2015 Storm." Journal of Geophysical Research: Space Physics 121, no. 6 (June 2016): 5537–5548 © 2016 American Geophysical Union

As Published: http://dx.doi.org/10.1002/2016JA022509

Publisher: American Geophysical Union (AGU)

Persistent URL: http://hdl.handle.net/1721.1/109263

Version: Final published version: final published article, as it appeared in a journal, conference proceedings, or other formally published context

AGU PUBLICATIONS

JGR

Journal of Geophysical Research: Space Physics

RESEARCH ARTICLE
10.1002/2016JA022509

Special Section:
Big Storms of the Van Allen Probes Era

Observations of the impenetrable barrier, the plasmapause, and the VLF bubble during the 17 March 2015 storm

J. C. Foster[1], P. J. Erickson[1], D. N. Baker[2], A. N. Jaynes[2], E. V. Mishin[3], J. F. Fennel[4], X. Li[2], M. G. Henderson[5], and S. G. Kanekal[6]

[1]Haystack Observatory, Massachusetts Institute of Technology, Westford, Massachusetts, USA, [2]Laboratory for Atmospheric and Space Physics, University of Colorado Boulder, Boulder, Colorado, USA, [3]Air Force Research Laboratory, Albuquerque, New Mexico, USA, [4]Space Sciences Laboratory, Aerospace Corp., Los Angeles, California, USA, [5]Los Alamos National Laboratory, Los Alamos, New Mexico, USA, [6]NASA Goddard Space Flight Center, Greenbelt, Maryland, USA

Key Points:
- A magnetically confined bubble of very low frequency (VLF) emissions of natural and human-produced origin surrounds the Earth
- The VLF bubble surrounding the Earth closely matches the position of the impenetrable barrier to the earthward extent of multi-MeV electrons
- VLF transmitter-induced waves act to sculpt the inner edge of MeV radiation belt electrons when large storms erode the plasmapause to L < 2.8

Correspondence to:
J. C. Foster,
jfoster@haystack.mit.edu

Citation:
Foster, J. C., P. J. Erickson, D. N. Baker, A. N. Jaynes, E. V. Mishin, J. F. Fennel, X. Li, M. G. Henderson, and S. G. Kanekal (2016), Observations of the impenetrable barrier, the plasmapause, and the VLF bubble during the 17 March 2015 storm, *J. Geophys. Res. Space Physics*, *121*, 5537–5548, doi:10.1002/2016JA022509.

Received 7 FEB 2016
Accepted 14 JUN 2016
Accepted article online 16 JUN 2016
Published online 30 JUN 2016

Abstract Van Allen Probes observations during the 17 March 2015 major geomagnetic storm strongly suggest that VLF transmitter-induced waves play an important role in sculpting the earthward extent of outer zone MeV electrons. A magnetically confined bubble of very low frequency (VLF) wave emissions of terrestrial, human-produced origin surrounds the Earth. The outer limit of the VLF bubble closely matches the position of an apparent barrier to the inward extent of multi-MeV radiation belt electrons near 2.8 Earth radii. When the VLF transmitter signals extend beyond the eroded plasmapause, electron loss processes set up near the outer extent of the VLF bubble create an earthward limit to the region of local acceleration near L = 2.8 as MeV electrons are scattered into the atmospheric loss cone.

1. Introduction

Earth is surrounded by a torus of relativistic electrons whose intensity, energy, and spatial extent vary dramatically with geomagnetic activity. This is the outer Van Allen radiation belt, located at radial distances ~3 to 6 Earth radii (R_E) and characterized by electron energies ranging from ~1 to 10 MeV or more.

Since their launch in late 2012, the Van Allen Probes [*Mauk et al.*, 2012] have contributed significantly to a new understanding of physical mechanisms involved in the loss and recovery of radiation belt electrons. During the first hours of strong geoeffective magnetic storms, the entire outer belt can be lost both to the atmosphere by wave scattering and to interplanetary space as greatly distorted drift orbits carry the electrons to the magnetopause [*Baker et al.*, 2013; *Ukhorskiy et al.*, 2015; *Jaynes et al.*, 2015]. Surprisingly, the MeV electron population can recover to previous or enhanced levels in a matter of hours [*Foster et al.*, 2014] to days [*Reeves et al.*, 2013]. Absent the impulsive effect of shocks [e.g., *Foster et al.*, 2015], the multi-MeV electron population can be replenished either through the slow process of inward diffusion and adiabatic acceleration or through the in situ acceleration of 100 s keV seed electrons to relativistic energies during interactions with very low frequency (VLF) chorus waves in the low-density region outside the eroded plasmapause [*Reeves et al.*, 2013; *Thorne et al.*, 2013; *Foster et al.*, 2014; *Baker et al.*, 2014a].

The recent study by *Baker et al.* [2014b] has noted that the earthward extent of the outer belt of highly relativistic electrons encounters a seemingly impenetrable barrier at an equatorial radial distance (L) near 2.8 R_E. Almost no electrons ≥ 2 MeV are seen inside this limiting position. In the inner radiation belt (L < 2.2), *Gamble et al.* [2008] found that interaction with VLF transmitter signals produces significant precipitation loss for electrons with energies <500 keV. Prior observations of this region [*Koons et al.*, 1981] combined with theory and modeling [*Abel and Thorne*, 1998] concluded that signals from ground-based VLF transmitters had no significant effect on relativistic electrons in the inner magnetosphere outside L ~ 2.4. *Baker et al.*'s [2014b] study suggested that the observed barrier for MeV electrons near 2.8 R_E can be maintained by an interplay of natural processes, in which very slow inward radial diffusion is balanced by slow but somewhat more rapid precipitation losses due to pitch angle diffusion driven by interactions with naturally occurring VLF hiss. In the current study we reexamine the effects of the VLF transmitters and augment *Baker et al.*'s [2014b] theory with an additional mechanism that keeps the barrier intact even during times of significant erosion of the plasmasphere.

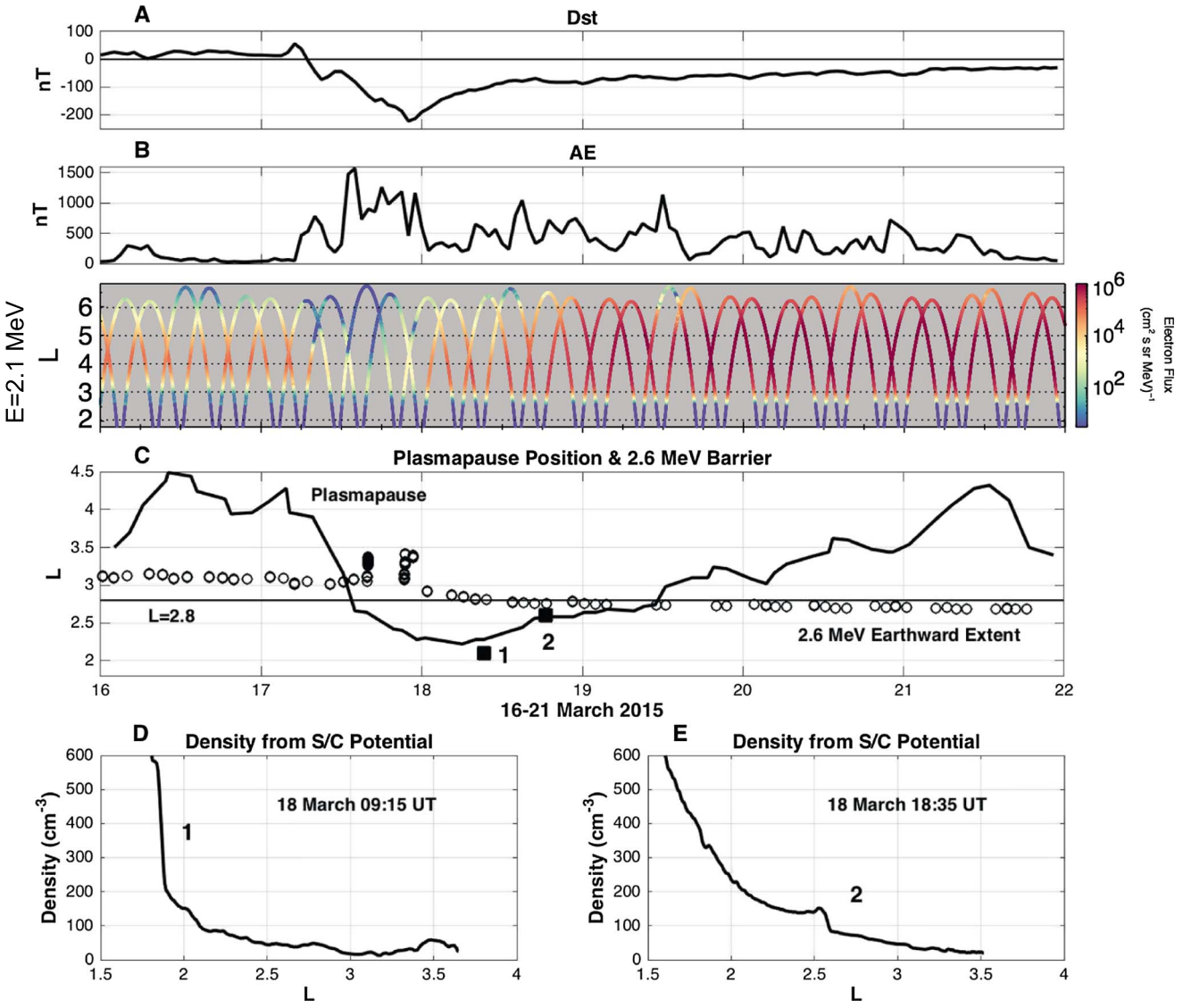

Figure 1. (a) Hourly *Dst* index is shown over the 6 day period 16-21 March 2015. Peak disturbance of this strong storm occurred early on 18 March. (b) One-hour averages of the *AE* index exceeded 1000 nT for the second half of 17 March. (c) The solid curve indicates a five-point running average of the radial position of the plasmapause determined from upper hybrid resonance line measurements with the EMFISIS HFR instrument by both spacecraft. The plasmapause was eroded from L ~ 4 to L ~ 2 during the first 24 h of the storm and was observed inside L = 2.8 for the entire UT day on 18 March. The position of the earthward extent of REPT 2.6 MeV electrons is indicated ("o"). Data from REPT A and B in an L versus time format with color indicating flux magnitude illustrating the rapid dropout and prompt recovery of 2.1 MeV outer zone electrons during the course of the storm are shown above. (d and e) Radial profiles of plasma density determined from EFW in situ measurements are shown for times (1) at the peak of the storm (18 March 09:15 UT, plasmapause eroded to L ~ 1.9) and (2) at the time of the observations of Figures 4–6 (18 March 18:30 UT) when the plasmapause had recovered to L ~ 2.6.

2. Observations

2.1. MeV Electron Gradients

One of the largest geomagnetic disturbances of the past decade began with the arrival of a solar wind shock at Earth and storm sudden commencement at ~04:45 UT on 17 March 2015. Minimum *Dst* index reached < -220 nT at ~23:00 UT, and by early on 18 March the plasmasphere had been eroded to L ~ 2 (Figure 1). This strong storm produced a rapid loss and subsequent prompt recovery of outer zone electrons (Figure 1, third panel) affording an excellent opportunity for investigating the barrier using the full complement of sensors carried by the Van Allen Probes. Following an initial severe depletion, the Relativistic Electron and Proton Telescope (REPT) [*Baker et al.*, 2012] observed a rapid and exceptionally strong recovery and enhancement of MeV outer zone electrons up to, but only outside, a sharply defined radial gradient near

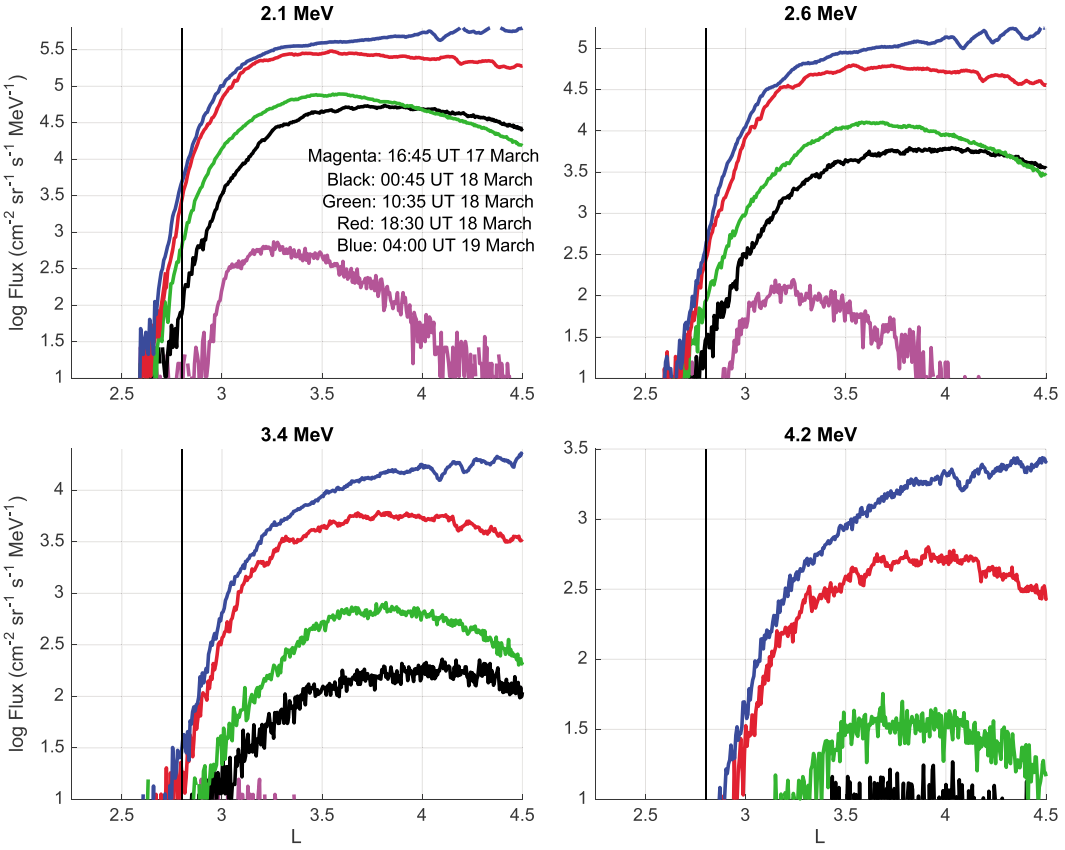

Figure 2. Van Allen Probe-A REPT observations in four relativistic electron flux channels are shown for successive outbound orbits over 30 h following the onset of the 17 March 2015 storm. The superposed radial profiles progressively approached an asymptotic limit near L ~ 2.8 where steep radial gradients were formed. This study presents a detailed analysis of conditions associated with the pass at 18:30 UT on 18 March 2015 (red profiles).

L ~ 2.8 (Figure 2). Lower energy electrons (10–100 s keV) observed with the Magnetic Electron Ion Spectrometer (MagEIS) [*Blake et al.*, 2013] penetrated inward of the barrier to L ~ 2 at the lowest energies. Electrons at these energies provide an energy source for VLF (chorus) wave amplification and a seed population for local acceleration to MeV energies [*Jaynes et al.*, 2015].

An examination of electron pitch angle distributions (see below) indicates a migration of MeV electron pitch angles toward the loss cone in the region of steep spatial gradients immediately outside the barrier at L ~ 2.8. Energetic electrons drift rapidly around the Earth as they bounce between magnetic mirror points in the northern and southern hemispheres. They are lost to atmospheric collisions preferentially in the southern hemisphere at the longitude of the South Atlantic magnetic anomaly, where their mirror altitude first dips below ~100 km. A mechanism providing a localized enhanced rate of pitch angle scattering around the L ~ 2.8 barrier could move freshly accelerated MeV electrons into either the local atmospheric or the drift loss cone, inhibiting radiation belt recovery inside this region and resulting in the rapid formation of the observed steep radial gradients in relativistic electrons.

The observations of both the steep flux gradients and the migration toward field-aligned pitch angles in the region immediately outside the barrier are strongly suggestive of a previously unrecognized fast acting (~1 day) and spatially localized (~0.5 R_E) mechanism responsible for the formation of these well-defined features during the active recovery of outer zone relativistic electrons.

2.2. The VLF Bubble

In addition to the highly sensitive REPT relativistic electron detectors, the Van Allen Probes carry a full complement of particle and wave instruments. These reveal strong signals from ground-based VLF transmitters in a striking spatial coincidence that implicates their involvement in the formation and maintenance of the

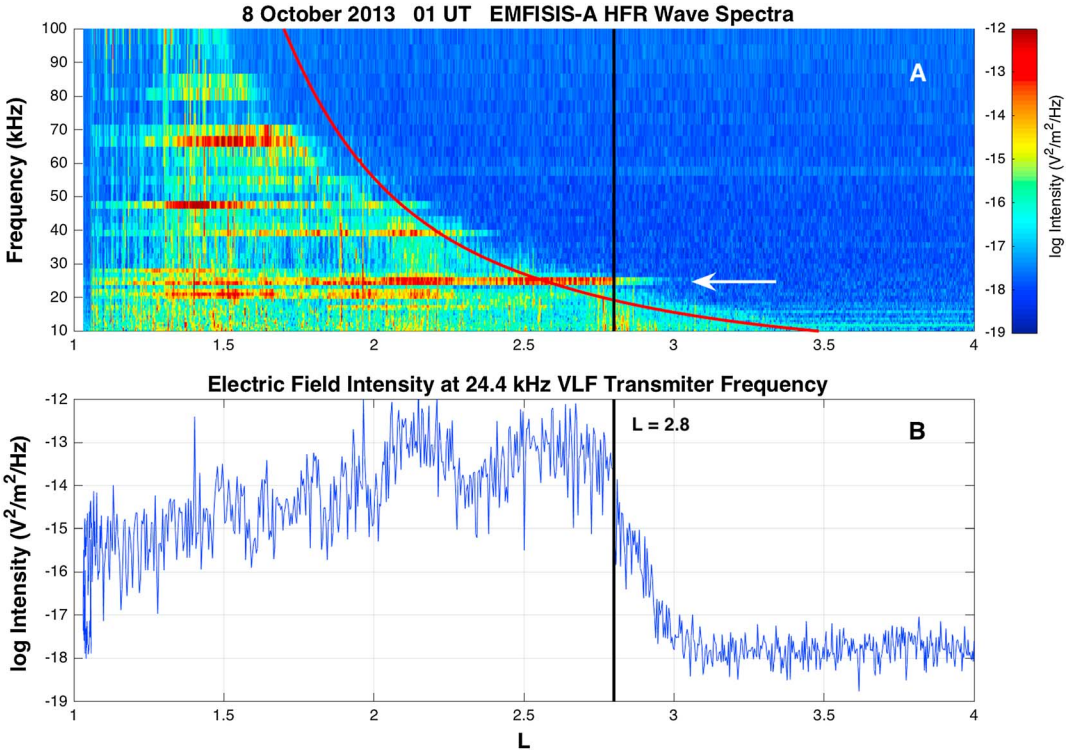

Figure 3. EMFISIS observations reveal the confinement of the signals from ground-based VLF transmitters to a magnetically confined bubble surrounding Earth. (a) Spectra of wave electric field intensity are plotted versus L for a perigee pass in October 2013 at a time when the plasmapause was beyond L = 4. The red curve denotes 0.5 f_{ce}. An arrow denotes the strong VLF transmitter signal near 24 kHz. (b) Electric field intensity ($|E|^2$) at the transmitter frequency increased by 10^5 over 0.5 R_E as Van Allen Probe A moved inward across the outer edge of the VLF bubble.

spatial gradient of the MeV electrons near L = 2.8. The Electric and Magnetic Field Instrument and Integrated Science (EMFISIS) wave instruments [*Kletzing et al.*, 2012] regularly observe a magnetically confined bubble of VLF emissions of terrestrial origin filling the inner magnetosphere (Figure 3). The strongest signals near 25 kHz are from U.S. Navy VLF radio stations that provide one-way communication to submarines in the Navy's fleet. A frequency-dependent outer extent of VLF whistler mode signals in the magnetosphere (i.e., a VLF bubble) is formed as ducted propagation of waves from lightning-induced whistlers or ground-based VLF transmitters is confined to L shells such that the wave frequency is ≤0.5 the minimum electron gyrofrequency (f_{ce}) along the field line [*Kulkarni et al.*, 2008]. Nonducted waves can propagate to the plasmapause in the transmitter hemisphere. There those signals build up along the caustic [*Starks et al.*, 2009], where the whistler wave can be transformed into a slowly moving oblique electrostatic wave with greatly increased amplitude.

For the outbound pass of Van Allen Probe-A near 18:30 UT on 18 March 2015, Figure 4 presents VLF wave observations across the full frequency range of the EMFISIS instruments along with details of the pitch angle distribution of the MeV electrons at the edge of the barrier. The location of the plasmapause near L ~ 2.6 is marked by the sharp drop in the frequency of the upper hybrid band waves near 100 kHz. For this pass, the strongest VLF transmitter signal occurred near 21.5 kHz and was significantly enhanced outside the plasmapause at the edge of the VLF bubble. Enhanced lower frequency emissions are also seen near the plasmapause, both around the lower hybrid resonance frequency (f_{LHR}, lower black line; yellow emissions above f_{LHR}) and between f_{LHR} and >2 proton gyrofrequencies (magnetosonic and ion Bernstein waves; red band). In Figure 4a, 2.1 MeV REPT electron fluxes exhibit pronounced butterfly normalized pitch angle distributions with flux maxima moving progressively toward smaller pitch angles between L = 3.2 and L = 2.8. A significant relative enhancement at smaller pitch angles is seen in the region between L = 2.85 and L = 3.0 during the disturbed storm interval, indicative of flux migration toward the loss cones immediately outside L = 2.8.

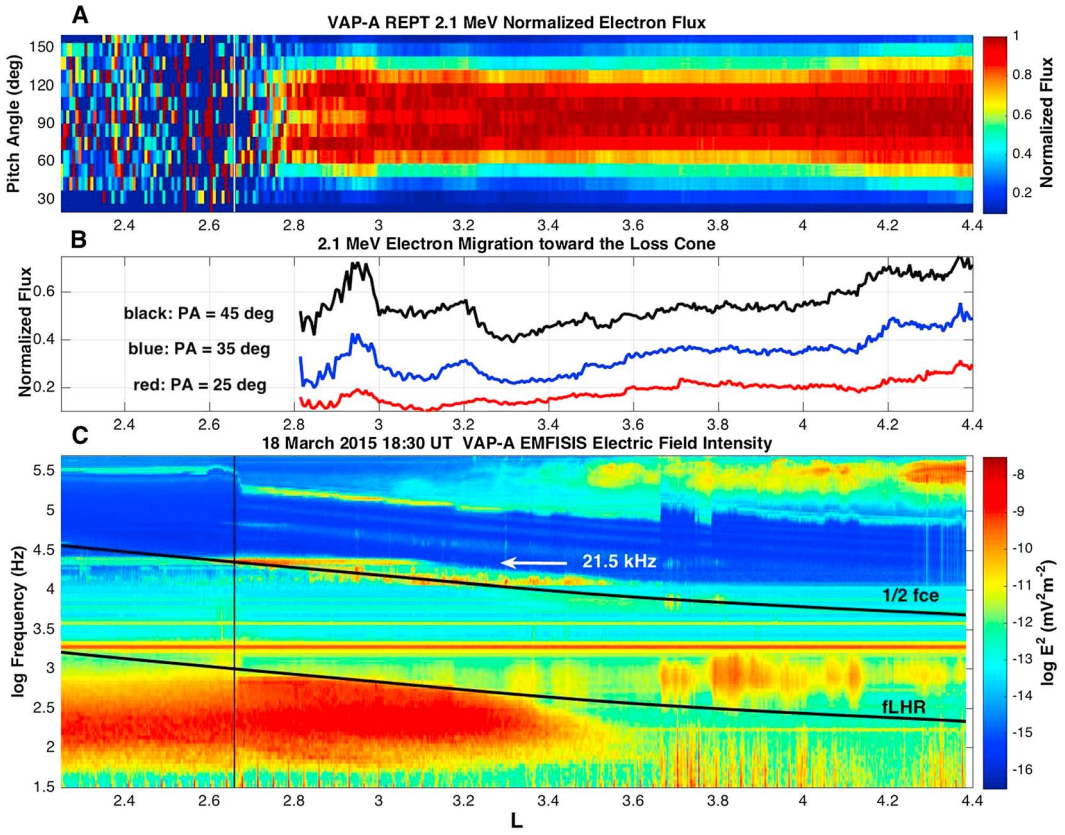

Figure 4. (a) Normalized pitch angle distributions for REPT 2.1 MeV electrons exhibit a pronounced butterfly distribution with peaks near 65° and 115° pitch angle inside L ~ 4. (b) Migration of the 2.6 MeV electron pitch angle distribution toward the atmospheric loss cone is seen in the spatially localized enhancement of normalized flux for off-equatorial mirroring electrons observed from L ~ 3.2 to L ~ 2.9. (c) EMFISIS electric field intensity spectra from 30 Hz to 500 kHz are shown with 0.5 f_{ce} and f_{LHR} denoted by sloping black lines. The plasmapause boundary is indicated by the vertical black line at L = 2.65. In the region where the ~21 kHz transmitter signal extends beyond the plasmapause, an enhancement of ion waves below f_{LHR} (~700 Hz) is observed.

The relationship of the strong VLF transmitter signal outside the eroded plasmapause to the sharp MeV electron flux gradients at the barrier is shown in Figure 5. During the 17 March 2015 event the 2.6 MeV electron flux decreased by 1000× across 0.5 R_E inside L = 3.2. Co-located with this electron decrease, VLF wave intensity at 21.5 kHz increased by 5 orders of magnitude across the outer boundary of the VLF bubble. We suggest that the observed 1000× increase in VLF electric field amplitude seen outside both the 0.5 f_{ce} boundary and the plasmapause is the effect of wave growth stimulated by the transmitter signal. Such interactions are significantly facilitated in the low electron density region outside the plasmapause [*Foster and Rosenberg*, 1976]. An ample energy source for the amplification of VLF emissions near the transmitter frequency was provided by abundant fluxes of 200 keV electrons observed by MagEIS (not shown) to extend earthward of the MeV electrons. Their anisotropic distribution is indicated by enhanced electron cyclotron harmonic waves at and below the upper hybrid frequency as seen in Figure 4.

2.3. The Plasmapause

Variations in plasma density strongly modulate the effectiveness of wave-particle interactions [*Inan et al.*, 1978] such that the position of the outer boundary of the comparatively dense plasmasphere is of considerable importance to the processes that shape the inner regions of the electron radiation belt. With Van Allen Probes observations we mark the position of the plasmapause using the variation of plasma density with L, as well as by the inward extent of ~100 eV O+ ions as observed by the Helium, Oxygen, Proton, and Electron (HOPE) mass spectrometer [*Funsten et al.*, 2013]. Plasma density is derived from the frequency of the upper hybrid resonance band, ω_{UH}, seen in EMFISIS HFR observations. Density versus L profiles also are obtained

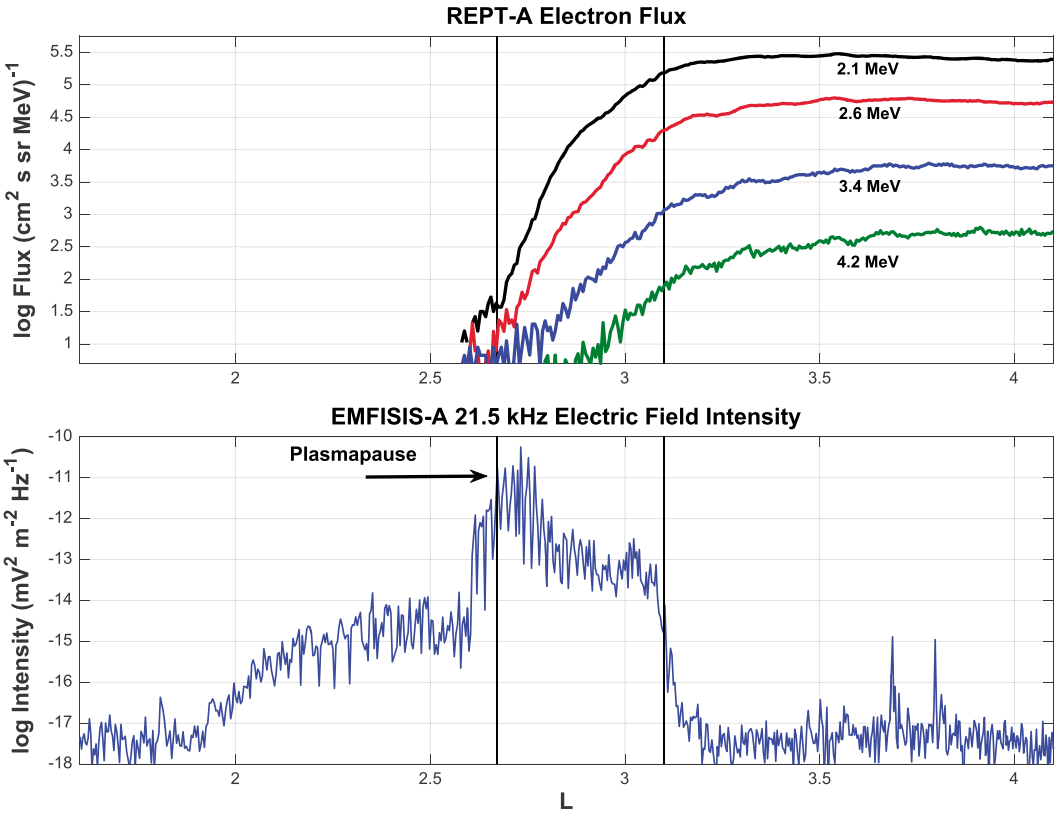

Figure 5. (a) REPT MeV electron fluxes at four energies exhibit sharp gradients outside the barrier. The 2.6 MeV flux decreases 1000-fold across 0.5 R_E. (b) Electric field wave intensity at the ~21 kHz transmitter frequency increases by $>10^5$ as the L decreases from 3.2 to 2.7. Enhanced wave power at VLF transmitter frequencies overlaps the region of steep gradient in MeV electron flux. The plasmapause position at L = 2.65 determined from the EMFISIS upper hybrid frequency and the outer extent of the enhanced VLF transmitter signal are indicated with black vertical lines.

through analysis of the electric field spin-plane boom potential differences observed with the Electric Field and Waves (EFW) instrument [*Wygant et al.*, 2013] and then calibrated during times of ideal plasma density measurements from ω_{UH}.

Figure 6 presents data sets demonstrating the close correspondence of three methods of plasmapause determination for 18:30 UT on 18 March 2015 across the range of L shown in Figure 5. Using a combination of the techniques described above, we have determined the position of the plasmapause through the interval 16–21 March 2015, and those results are presented in Figure 1c. Plasmasphere erosion during the early phases of the storm erodes the plasmapause to L < 2 by 12:00 UT on 18 March. The plasmapause then recovered to L ~ 3 by early on 19 March. The relationship of the plasmapause to the inner extent of relativistic electrons (the impenetrable barrier) is shown in Figure 1c for times spanning the period during which the strong spatial gradients of Figure 2 were formed. Despite the location of the plasmapause's well inside L = 2.8, and the evidence for strong local MeV electron acceleration in the rapidly recovering outer radiation belt, the earthward extent of 2.6 MeV electron fluxes remained outside L = 2.8 throughout the interval. Radial profiles of plasma density determined from EFW measurements are shown in Figures 1d and 1e for times at the peak of the storm when the plasmapause had eroded to L ~ 1.9 (09:15 UT; labeled "1") and at the time of the observations of Figure 5 when the plasmapause had recovered to L ~ 2.6 (18:35 UT, labeled "2").

3. Wave-Particle Interactions Outside the Plasmapause

3.1. Cyclotron Resonance

Previous modeling studies have investigated the effects of VLF transmitters on the outer zone electrons based on quasi-linear diffusion calculations. Using ambient densities of ~1000 cm^{-3} at L = 2.8, appropriate to the inner

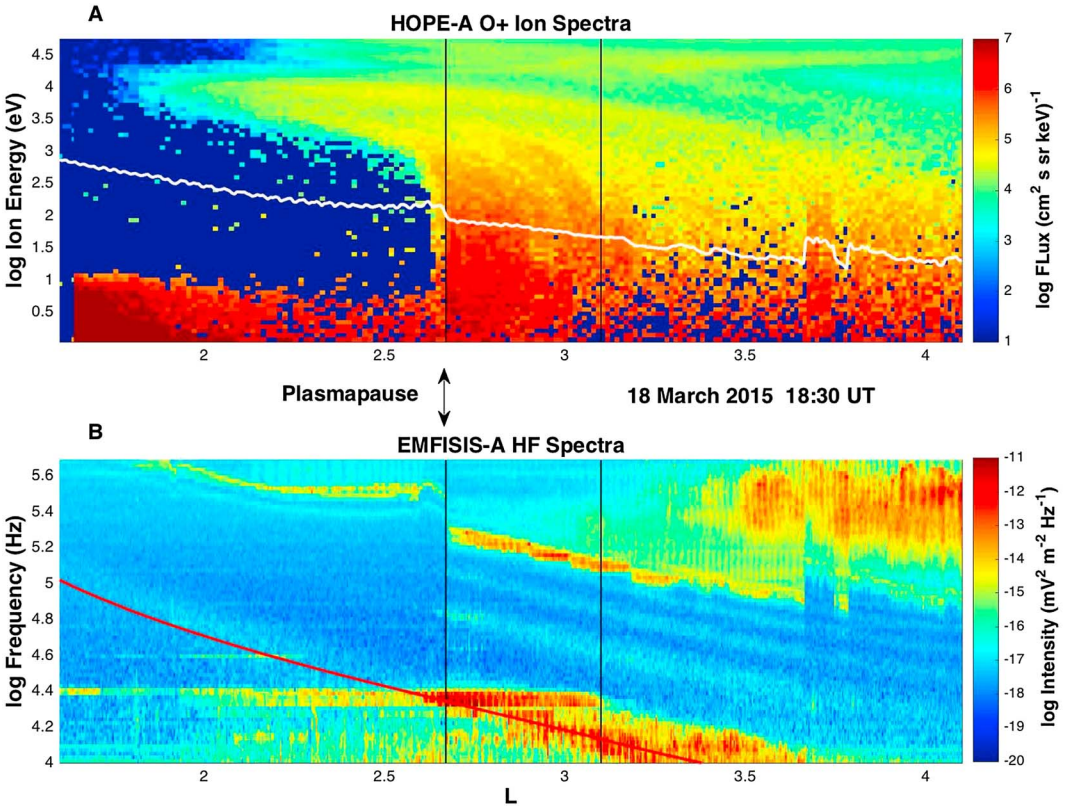

Figure 6. Three methods of determining the plasmapause position are shown. (a) At ion energies ~100 eV, HOPE oxygen energy spectra show a sharp inner boundary (method 1) at the plasmapause at L = 2.65. A pronounced "nose" of >1 keV oxygen ions extends inward of the plasmapause. In situ EFW boom potential difference measurements of cold plasma density are superimposed on the ion spectra (white curve plotted on the ion energy log scale). The plasmapause density gradient (method 2) is seen at L = 2.65. (b) EMFISIS high-frequency electric field intensity spectra are shown with 0.5 f_{ce} denoted by a red line. Plasma density and plasmapause location are obtained from the frequency of the upper hybrid resonance band (method 3). The VLF transmitter signal significantly increases in intensity as it encounters a band of natural chorus emissions at 0.5 f_{ce} immediately beyond the plasmapause. Narrowband emissions above f_{ce} (electron Bernstein modes) indicate the unstable low-energy electron population outside the plasmapause.

plasmasphere, those studies concluded that there is little interaction of 20 kHz VLF waves with MeV electrons outside L = 2.6 [*Abel and Thorne*, 1998; *Kulkarni et al.*, 2008]. Less attention has been paid to the effects of nonlinear interactions [*Abel and Thorne*, 1998], although their possible effect has been noted [*Inan et al.*, 1978; *Albert*, 2002].

The general equation for electron cyclotron resonance is

$$\omega - k_{par} v_{par} = -n \ \omega_{ce}/\gamma$$

where ω is the wave frequency, k_{par} and v_{par} are the components of the wave number and the electron velocity parallel to the magnetic field line, n is the harmonic resonance number, ω_{ce} is the electron gyrofrequency, and γ is the relativistic Lorentz factor [*Abel and Thorne*, 1998]. The energy of electrons resonant with a wave of a given frequency is strongly dependent on magnetic field strength, electron pitch angle, and plasma density in the interaction region.

3.2. Resonant Electron Energy

The significant change in cyclotron resonance conditions associated with the much lower densities outside an eroded plasmasphere is demonstrated in Figure 7. The L-space profiles of the energy of electrons resonant with 21 kHz and 700 Hz (near f_{LHR}) waves are shown for equatorial electron density profiles representative of extended and eroded plasmasphere conditions based on March 2015 observations by the Van Allen Probes spacecraft and using a dipole magnetic field configuration, The density profiles are shown in Figure 7a. Figure 7b presents resonance conditions between 21 kHz waves and MeV electrons possessing butterfly

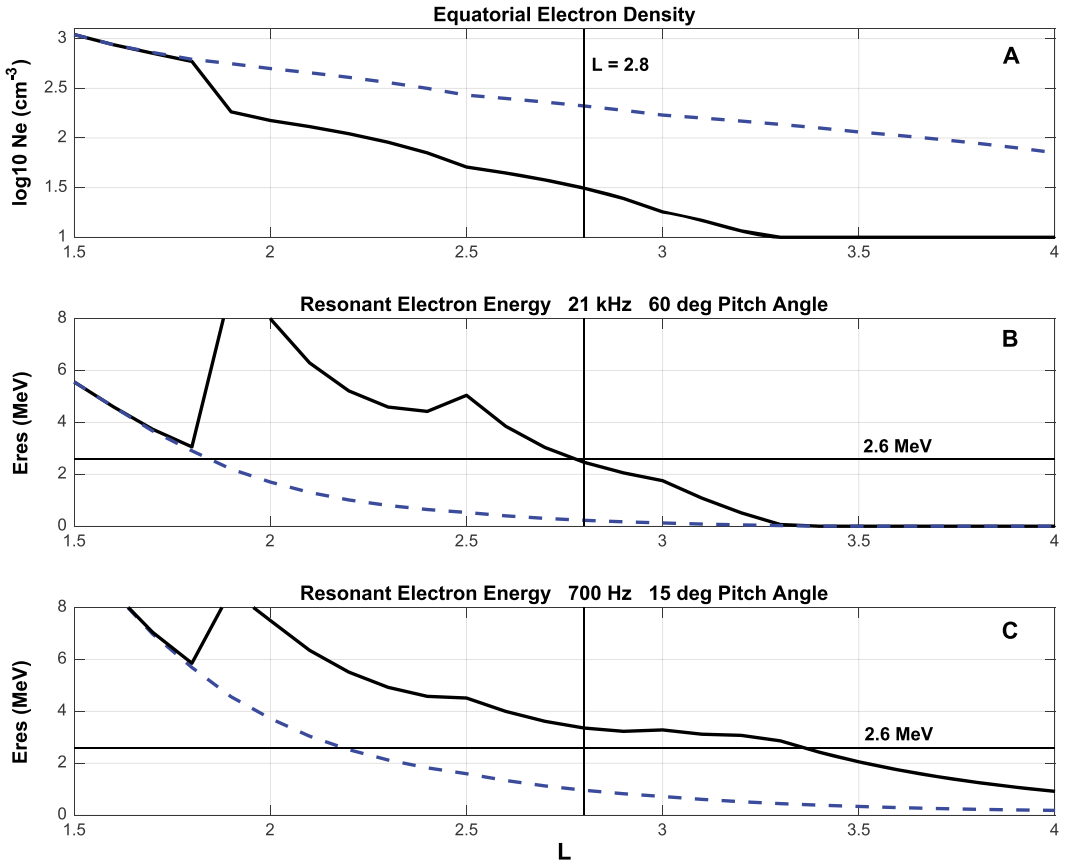

Figure 7. L-space profiles of the energy of electrons resonant with 21 kHz and 700 Hz waves are shown for equatorial electron density profiles representative of extended and eroded plasmasphere conditions. (a) Density profiles derived from representative Van Allen Probes observations during March 2015 are shown for extended (dashed) and eroded (solid curve) plasmasphere conditions. (b) For 21 kHz waves, resonant energies of MeV electrons with butterfly pitch angle distributions peaked near 60 deg are shown for the two density profiles shown in Figure 7a. Multi-MeV electrons at L ~ 2.8 are in resonance with VLF waves at the transmitter frequency for the eroded plasmasphere (solid curve). (c) For 700 Hz waves, multi-MeV electrons with small pitch angles are in resonance ($n = -1$) at L ~ 2.8 when the plasmasphere is eroded.

pitch angle distributions peaked near 60° (cf. Figure 4). The strong dependence of electron resonant energy on ambient cold plasma density is seen across the sharp density gradient at the plasmapause (L ~ 1.9 in Figures 7b and 7c). In the low-density region outside the eroded plasmapause, MeV electrons at L = 2.8 at the edge of the VLF bubble are in primary cyclotron resonance ($n = -1$) with waves at the 21 kHz transmitter frequency. At pitch angles closer to the loss cone, the abundant ~100 keV electrons resonate with 21 kHz waves (not shown) and can provide a significant energy source for the observed wave amplification around the transmitter frequency. Figure 7c demonstrates that multi-MeV electrons at L ~ 2.8 are in resonance ($n = -1$) with 700 Hz waves at small pitch angles when the plasmasphere is eroded. These interactions have the potential to accelerate MeV electron losses in this region through scattering into the atmospheric loss cone.

For the conditions observed in the March 2015 storm we suggest that the effect of the VLF transmitter signal involves a multistep process of transmitter-induced interactions with several magnetospheric particle populations leading to signal amplification, wave mode conversion, and enhanced migration of multi-MeV electrons into the loss cone. Details of the proposed interactions and a schematic representation of the waves, electron populations, and processes involved are presented in Appendix A.

4. Discussion

The observations reported here strongly suggest that VLF transmitter-induced waves play an important role in sculpting the inner edge of the freshly accelerated electrons during large storms when VLF signals near

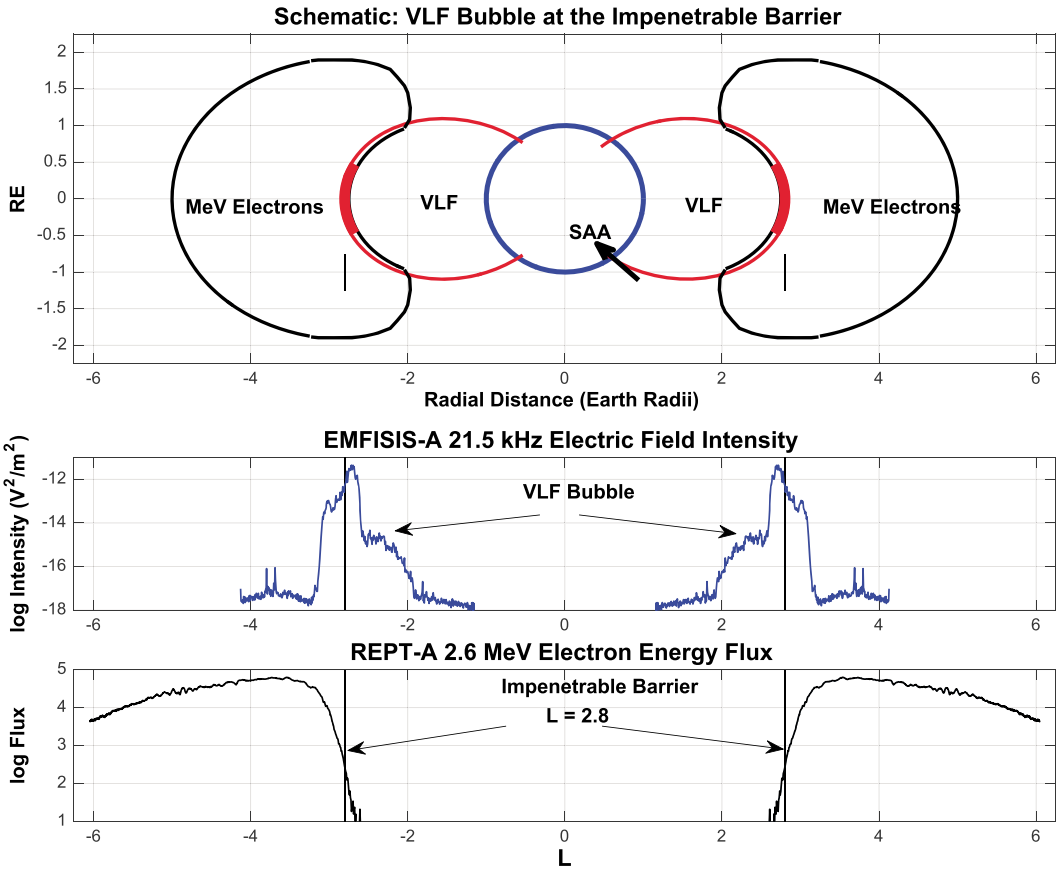

Figure 8. Schematic representing the overlap of the inner edge of the electron radiation belt with the strong VLF transmitter signals at the outer edge of the VLF bubble in the region surrounding Earth. The L-space profiles of VLF transmitter signal intensity and 2.6 MeV electron flux observed during the 18:30 UT 18 March pass of Probe A are shown.

20 kHz extend beyond the eroded plasmapause. During these conditions, localized MeV electron loss processes set up near the outer extent of the VLF bubble create an earthward limit to the region of local acceleration near L = 2.8 as MeV electrons are scattered into the atmospheric loss cone. The observations and effects reported here are not unique. Wave and particle characteristics observed during the 23–25 June 2015 major storm are closely similar to those seen during the March 2015 event (cf. Figure 4). Based on March 2015 observations, the schematic picture shown in Figure 8 represents the overlap of the inner edge of the electron radiation belt with the strong VLF transmitter signals at the outer edge of the VLF bubble in the region surrounding Earth. The VLF bubble and the outward extent of the transmitter signals are fixed in space near L ~ 2.8 by the relative invariance of Earth's magnetic field.

The study adds to the current theoretical picture of the formation of the barrier as described in *Baker et al.* [2014b]. The suggested interdependence of the location of the impenetrable barrier with the outward extent of the VLF transmitter signals and the plasmapause position suggests that the relativistic electron barrier can be maintained even when storm conditions are strong enough to erode the plasmapause inward of the barrier region.

This study also raises a number of questions for further investigation. The plasma processes involved need further specification and clarification. Obtaining quantitative estimates for the effects we propose here may necessitate the development of models including of nonlinear processes. Using current quasi-linear models of the interaction of VLF transmitter signals with MeV electrons, the wave amplitudes observed by Van Allen Probes do not appear to be large enough to result in strong precipitation. However, the true intensity of the short-wavelength (1–50 m) 21 kHz near-electrostatic waves likely is underestimated observationally by a factor of 50 to several hundreds or more due to a mismatch with the characteristics of the 100 m EFW antenna [*Wygant et al.*, 2013] used to measure this frequency band. There is also some indication in this event

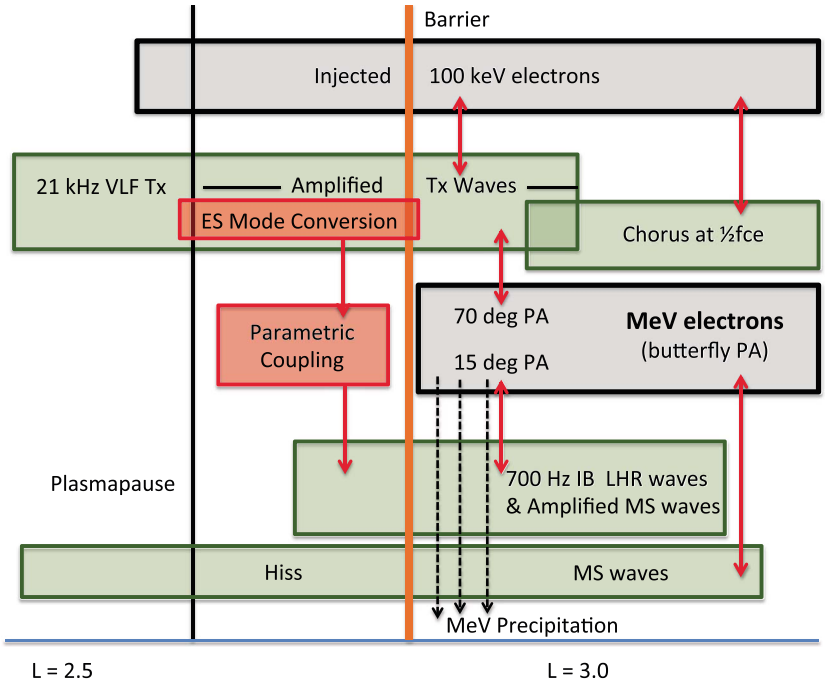

Figure A1. Schematic representation of the spatial extent and interrelationships of waves and electrons in the vicinity of the impenetrable barrier during the March 2015 event are shown based on the observations of Figure 4. The approximate extent of the VLF transmitter signal (Tx) and waves in the lower hybrid resonance (LHR), ion Bernstein (IB), magnetosonic (MS), and hiss populations are shown in green. Electron populations are indicated in black. Interactions between specific wave and electron populations are shown with red arrows, and wave mode conversion and wave-wave interactions are indicated in the red boxes. (See text for descriptions of the processes involved.)

(cf. Figure 4) that natural chorus band emissions at frequencies below 0.5 f_{ce} may have been suppressed at the edge of the VLF bubble (L ~ 2.8). These discrete chorus rising tones are important in the local acceleration of MeV electrons [e.g., *Omura et al.*, 2015].

The observed energy dependence of the barrier location also needs further improvements in understanding. Whereas the ~2 MeV electrons moved in some strength below L ~ 2.8 following the 17 March storm, the higher energy electrons do not breach the L ~ 2.8 barrier location. The observed outer zone gradients and flux levels in this early recovery period are interrelated functions of particle injection, local acceleration, inward diffusion, wave-particle resonances, and localized processes. These processes have strong dependences on the energies and preexisting spatial particle distributions, in addition to ambient cold plasma density and magnetic field strength. The interrelationships of these processes pose interesting further questions to be addressed in later studies. It is important to understand whether some variants of the mechanism involving the VLF transmitters are operative in maintaining the characteristics of the barrier even when the plasmapause is far outside its location. Finally, it seems possible that different processes are operative during the initial establishment of the barrier and during its subsequent maintenance and evolution.

Appendix A: Mode Conversion and Parametric Coupling

A schematic representation of the spatial extent and interrelationships of waves and electrons in the vicinity of the impenetrable barrier during the March 2015 event is presented in Figure A1.

In addition to amplification by an unstable distribution of 100 s keV electrons, indicated in the wave observations of Figure 6 by the electron cyclotron harmonics outside the plasmapause, the transmitted whistler wave may experience mode conversion in the resonance region, as follows. The dispersion relation of an oblique whistler wave in cold plasma is expressed as $\frac{k^2c^2}{\omega^2} = 1 - \frac{\omega_{pe}^2}{\omega(\omega-\omega_{ce}\cos\vartheta)}$, where ω_{pe}/ω_{ce} is the electron plasma/cyclotron frequency and $\cos\vartheta = k_{\|}/k$. The frequency of electrostatic waves is $\omega = \omega_{ce}\cos\vartheta$ at $\omega \ll \omega_{ce}$ and $\cos^2\vartheta \gg m_e/m_i$, where m_e/m_i is the electron/ion mass. When the whistler frequency ω approaches $\omega_{ce}\cos\vartheta$,

the wave becomes quasi-electrostatic ($kc/\omega \to \infty$) and has a resonance cone character. Near the resonance cone, especially when perpendicular density gradient (plasmapause) is present, a whistler wave is effectively transformed into a slowly moving oblique electrostatic wave with the greatly increased amplitude.

Both whistler and oblique electrostatic wave modes are known to be parametrically coupled with the lower frequency electrostatic sideband $\omega_1 = \omega - \Omega$, where Ω is the frequency of lower hybrid (LH) or ion Bernstein (IB) modes [*Porkolab*, 1978]. Parametric interactions lead to broadening of the initially narrow signal over multiple LH or IB frequencies and generation of the corresponding LH (IB) wave band limited from below (above) by the lower hybrid resonance ω_{lhr}. Generally speaking, the same approach is applicable to parametric interactions with magnetosonic waves that have virtually the same spectrum as the IB band. Another well-known outcome of the parametric instability is heating of plasma particles consistent with the superthermal (tens of eV) O+ ion population outside the plasmapause at the edge of the VLF bubble.

The nose-like ion distribution seen in Figure 6 inside the plasmasphere is typical for ring current injections on the duskside and known to excite LH and magnetosonic waves near the magnetic equator via an ion-ring instability [*Mishin and Burke*, 2005; *Horne et al.*, 2007; *Mishin et al.*, 2011]. Another source acting in the plasmaspheric boundary layer is the lower hybrid drift instability driven by the diamagnetic drift of hot electrons arrested at the plasmapause [*Mishin*, 2013]. In contrast, the broad ion distribution outside the plasmasphere does not appear to be unstable. The observed fast magnetosonic waves (Figure 4) and O+ ions (Figure 6) have different distributions inside and outside the plasmasphere. The magnetosonic-like wave band below f_{LHR} collocated with the signal increase at the VLF transmitter frequency is more enhanced than its counterpart inside the plasmapause. This suggests that the outside band is a consequence of the aforementioned parametric interactions.

Acknowledgments

We thank W. Kurth for input concerning the EMFISIS wave observations, J. Bonnell for discussions of EFW antenna sensitivity, M. Starks for guidance on VLF propagation characteristics, and J. Albert for helpful discussions and for providing the relativistic electron resonance code used in Figure 7. J.C.F. and P.J.E. received support from a University of Minnesota subcontract award to the Massachusetts Institute of Technology. E.M. was supported by the Air Force Office of Scientific Research. Van Allen Probes data access was provided through the Johns Hopkins University/Applied Physics Lab Mission Operations Center and the Los Alamos National Laboratory Science Operations Center. This work was supported by JHU/APL contract 967399 under NASA's prime contract NAS5-01072. All Van Allen Probes data used are publicly available at (www.rbsp-ect.lanl.gov).

References

Abel, B., and R. M. Thorne (1998), Electron scattering loss in Earth's inner magnetosphere 1. Dominant physical processes, *J. Geophys. Res.*, *103*, 2385–2396, doi:10.1029/97JA02919.

Albert, J. M. (2002), Nonlinear interaction of outer zone electrons with VLF waves, *Geophys. Res. Lett.*, *29*(8), 1275, doi:10.1029/2001GL013941.

Baker, D. N., et al. (2012), The Relativistic Electron-Proton Telescope (REPT) instrument on board the Radiation Belt Storm Probes (RBSP) spacecraft: Characterization of Earth's radiation belt high-energy particle populations, *Space Sci. Rev.*, doi:10.1007/s11214-012-9950-9.

Baker, D. N., et al. (2013), A long-lived relativistic electron storage ring embedded in Earth's outer Van Allen belt, *Science*, *340*, 186–190, doi:10.1126/science.1233518, Medline.

Baker, D. N., et al. (2014a), Gradual diffusion and punctuated phase space density enhancements of highly relativistic electrons: Van Allen Probes observations, *Geophys. Res. Lett.*, *41*, 1351–1358, doi:10.1002/2013GL058942.

Baker, D. N., et al. (2014b), An impenetrable barrier to ultrarelativistic electrons in the Van Allen radiation belts, *Nature*, *515*, 7528, doi:10.1038/nature13956.

Blake, J. B., et al. (2013), Magnetic Electron Ion Spectrometer (MagEIS) instruments aboard the Radiation Belt Storm Probes (RBSP) spacecraft, *Space Sci. Rev.*, doi:10.1007/s11214-013-9991-8.

Foster, J. C., and T. J. Rosenberg (1976), Electron precipitation and VLF emissions associated with cyclotron resonance interactions near the plasmapause, *J. Geophys. Res.*, *81*, 2183–2192, doi:10.1029/JA081i013p02183.

Foster, J. C., et al. (2014), Prompt energization of relativistic and highly relativistic electrons during a substorm interval: Van Allen Probes observations, *Geophys. Res. Lett.*, *41*, 20–25, doi:10.1002/2013GL058438.

Foster, J. C., J. R. Wygant, M. K. Hudson, A. J. Boyd, D. N. Baker, P. J. Erickson, and H. E. Spence (2015), Shock-induced prompt relativistic electron acceleration in the inner magnetosphere, *J. Geophys. Res. Space Physics*, *120*, 1661–1674, doi:10.1002/2014JA020642.

Funsten, H. B., et al. (2013), Helium, Oxygen, Proton, and Electron (HOPE) mass spectrometer for the Radiation Belt Storm Probes Mission, *Space Sci. Rev.*, *179*, 423–484, doi:10.1007/s11214-013-9968-7.

Gamble, R. J., C. J. Rodger, M. A. Clilverd, J.-A. Sauvaud, N. R. Thomson, S. L. Stewart, R. J. McCormick, M. Parrot, and J.-J. Berthelier (2008), Radiation belt electron precipitation by man-made VLF transmissions, *J. Geophys. Res.*, *113*, A10211, doi:10.1029/2008JA013369.

Horne, R. B., R. M. Thorne, S. A. Glauert, N. P. Meredith, D. Pokhotelov, and O. Santolík (2007), Electron acceleration in the Van Allen radiation belts by fast magnetosonic waves, *Geophys. Res. Lett.*, *34*, L17107, doi:10.1029/2007GL030267.

Inan, U. S., T. F. Bell, and R. A. Helliwell (1978), Nonlinear pitch angle scattering of energetic electrons by coherent VLF waves in the magnetosphere, *J. Geophys. Res.*, *83*, 3235–3253, doi:10.1029/JA083iA07p03235.

Jaynes, A. N., et al. (2015), Source and seed populations for relativistic electrons: Their roles in radiation belt changes, *J. Geophys. Res. Space Physics*, *120*, 7240–7254, doi:10.1002/2015JA021234.

Kletzing, C. A., et al. (2012), The Electric and Magnetic Field Instrument and Integrated Science (EMFISIS) on RBSP, *Space Sci. Rev.*, doi:10.1007/s11214-013-99.

Koons, H. C., B. C. Edgar, and A. L. Vampola (1981), Precipitation of inner zone electrons by whistler mode waves from the VLF transmitters UMS and NWC, *J. Geophys. Res.*, *86*, 640–648, doi:10.1029/JA086iA02p00640.

Kulkarni, P., U. S. Inan, T. F. Bell, and J. Bortnik (2008), Precipitation signatures of ground-based VLF transmitters, *J. Geophys. Res.*, *113*, A07214, doi:10.1029/2007JA012569.

Mauk, B. H., N. J. Fox, S. G. Kanekal, R. L. Kessel, D. G. Sibeck, and A. Ukhorskiy (2012), Science objectives and rationale for the Radiation Belt Storm Probes mission, *Space Sci. Rev.*, doi:10.1007/s11214-012-9908-y.

Mishin, E. V. (2013), Interaction of substorm injections with the subauroral geospace: 1. Multispacecraft observations of SAID, *J. Geophys. Res. Space Physics*, *118*, 5782–5796, doi:10.1002/jgra.50548.

Mishin, E. V., and W. J. Burke (2005), Stormtime coupling of the ring current, plasmasphere, and topside ionosphere: Electromagnetic and plasma disturbances, *J. Geophys. Res.*, *110*, A07209, doi:10.1029/2005JA011021.

Mishin, E., J. Albert, and O. Santolik (2011), SAID/SAPS-related VLF waves and the outer radiation belt boundary, *Geophys. Res. Lett.*, *38*, L21101, doi:10.1029/2011GL049613.

Omura, Y., Y. Miyashita, M. Yoshikawa, D. Summers, M. Hikishima, Y. Ebihara, and Y. Kubota (2015), Formation process of relativistic electron flux through interaction with chorus emissions in the Earth's inner magnetosphere, *J. Geophys. Res. Space Physics*, *120*, 9545–9562, doi:10.1002/2015JA021563.

Porkolab, M. (1978), Parametric processes in magnetically confined CTR plasmas, *Nucl. Fusion*, *18*, 367.

Reeves, G. D., et al. (2013), Electron acceleration in the heart of the Van Allen radiation belts, *Sciencexpress*, doi:10.1126/science.1237743.

Starks, M. J., T. F. Bell, R. A. Quinn, U. S. Inan, D. Piddyachiy, and M. Parrot (2009), Modeling of Doppler- shifted terrestrial VLF transmitter signals observed by DEMETER, *Geophys. Res. Lett.*, *36*, L12103, doi:10.1029/2009GL038511.

Thorne, R. M., et al. (2013), Rapid local acceleration of relativistic radiation-belt electrons by magnetospheric chorus, *Nature*, *504*, 411–414, doi:10.1038/nature12889.93-.

Ukhorskiy, A. Y., M. I. Sitnov, R. M. Millan, B. T. Kress, J. F. Fennell, S. G. Claudepierre, and R. J. Barnes (2015), Global storm-time depletion of the outer electron belt, *J. Geophys. Res. Space Physics*, *120*, 2543–2556, doi:10.1002/2014JA020645.

Wygant, J. R., et al. (2013), The Electric Field and Waves (EFW) instruments on the Radiation Belt Storm Probes Mission, *Space Sci. Rev.*, doi:10.1007/s1124-013-0013-7.